Journal of Molecular Liquids 339 (2021) 116732

Contents lists available at ScienceDirect

Journal of Molecular Liquids

journal homepage: www.elsevier.com/locate/molliq

Adsorption behavior of uracil on external surface of MgO nanotubes: A new class of hybrid nano-bio materials

Yan Cao [a], Afrasyab Khan [b], M. Javan [c], Mohammad T. Baei [d], Elham Tazikeh-Lemeski [e,*], Zivar Azmoodeh [f], Alireza Soltani [g,*], Fatemeh Heidari [h], Marieh Pishnamazi [i], Ahmad B. Albadarin [j]

[a] School of Mechatronic Engineering, Xi'an Technological University, Xi'an 710021, China
[b] Institute of Engineering and Technology, Department of Hydraulics and Hydraulic and Pneumatic Systems, South Ural State University, Lenin Prospect 76, Chelyabinsk 454080, Russian Federation
[c] Department of Physics, Faculty of Sciences, Golestan University, Gorgan, Iran
[d] Department of Chemistry, Azadshahr Branch, Islamic Azad University, Azadshahr, Golestan, Iran
[e] Department of Chemistry, Gorgan Branch, Islamic Azad University, Gorgan, Iran
[f] Young Researchers and Elite Club, Behshahr Branch, Islamic Azad University, Behshahr, Iran
[g] Golestan Rheumatology Research Center, Golestan University of Medical Science, Gorgan, Iran
[h] Cancer Research Center, Golestan University of Medical Sciences, Gorgan, Iran
[i] Department of Chemistry, Arak Branch, Islamic Azad University, Arak, Iran
[j] Department of Chemical Sciences, Bernal Institute, University of Limerick, Limerick, Ireland

ARTICLE INFO

Article history:
Received 3 May 2021
Revised 3 June 2021
Accepted 13 June 2021
Available online 16 June 2021

Keywords:
MgONT
Uracil
UV-Vis spectroscopy
Photoinjection
Biochemical sensor

ABSTRACT

In this study, geometries, binding, optical and electronic features and charge-transfer characteristics of magnesium oxide nanotubes (MgONTs) interacting with uracil pyrimidine were evaluated in both vacuum and solvent (water and toluene) environments by using density functional theory (DFT) and time-dependent density functional theory (TDDFT) calculations. The binding energy of uracil was estimated to be in a range of −0.543 to −1.864 eV in vacuum, −0.347 to −1.709 eV in toluene, and −0.193 to −1.592 eV in water environments. Furthermore, the values of the binding and reaction energies are all negative meaning that the binding of uracil on MgONT is energetically favorable and the synthesis of the complex structure is possible. The results illustrate that the adsorption energy values of uracil on MgONT also follow the order of vacuum > toluene > water. Our analysis demonstrates that solvent polarity is so significant on the stability and reactivity of uracil. In contrast to vacuum and toluene environments, the dipole moment value of MgONT in water environment was significantly increased upon adsorption of uracil. Our findings illustrate that MgONT was more sensitive for detecting the uracil in vacuum environment than water and toluene environments to exploit as a biochemical sensor.

1. Introduction

Recently, the vast technologically momentous applications of amino acids, nucleic acids, peptides, and proteins adsorbed on the surface of metal oxides, particularly in photonics, microelectronics, heterogeneous catalysts, and photovoltaic devices, have reported efficient and important fundamental studies of adsorption of biomolecules on metal oxide nanostructures [1–6]. Surface interactions between nanostructures and nucleobases molecules or amino acids were found to be extremely useful as principal subjects in sensing, bioengineering, and nanoelectronics [7-13]. Uracil ($C_4H_4N_2O_2$) is a small molecule and is one of the four nucleobases in the nucleic acid of ribonucleic acid (RNA) that consists of two N-H and two carbonyl groups, one C = C double bond, and may ergo interacting with the surface in different ways [14]. Therefore, the junction of nucleic acid and metal oxides would contain features which make it very appealing for a vast range of unforeseen applications [15,16]. Here, we evaluated theoretical methods based on DFT and TDDFT to study the interaction between the RNA pyrimidine uracil and MgO nanotube to describe the changes of the structural, electronic, and optical properties on the nanotube. The MgO (1 0 0) structure is one of the most well-investigated oxide surfaces. It has been especially momentous in adsorption studies of small molecules on oxide surfaces [17-19]. A recent report indicates that MgO nanoparticles have no toxicity for cell lines, and shows potential applications in nanomedicine as a diagnostic and

* Corresponding authors.
E-mail addresses: elham.tazikeh@gmail.com (E. Tazikeh-Lemeski), alireza.soltani46@yahoo.com, alireza.soltani@goums.ac.ir (A. Soltani).

https://doi.org/10.1016/j.molliq.2021.116732
0167-7322/

therapeutic tool [20]. Newly, the MgO nano-particles are used for applications in tumor treatment and also it is known as an antibacterial agent [21]. The selections of MgO nanostructures as a suitable material for biosensor applications in the interaction with nucleobases are interesting because of the biocompatibility and effective surface area [22,23]. MgO nanoparticles have capability to destroy cancer cells and explained the reason of cell death because of MgO exposure [24]. Recently, Fornaro *et al.* experimentally showed that MgO acts as a good adsorbent for the adsorption of the nucleobases adenine and uracil in comparison to cytosine and hypoxanthine [25]. Rajarajeswari *et al.* have been shown uracil adsorption on single-walled carbon nanotubes (SWCNTs) in the presence of toluene molecules using DFT calculations [26]. In the previous study, we calculated the adsorption of uracil upon the surface of boron nitride (BN) and aluminium nitride (AlN) nanocages using DFT method [27]. Sharma and Kakkar have found a strong interaction for sarin with the perfect and Ti-doped MgONTs by DFT calculation. They also found that doping with Ti atom leads to improvement the structural and electronic features of MgONT [28]. Yang and co-workers have been investigated adsorption of CO upon TM-doped MgO nanotubes (TM = Ni, Pd and Pt) by using DFT calculations [29]. They have shown high adsorption energy of 1.61 and 2.55 eV for CO adsorbed on Pd and Pt-doped MgO nanotubes. Gowtham *et al.* studied the interaction of the adenine (A), cytosine (C), guanine (G), thymine (T), and uracil (U) over single-walled carbon nanotubes (SWCNTs) using Vienna Ab initio Simulation Package (VASP). They found that interaction from different chirality may affect the binding energy of nucleic acid bases with high-curvature CNTs [30]. The biosensing applications of graphene and boron nitride graphene on nucleic acid bases (Adenine, Cytosine, Guanine, Thymine, and Uracil) were evaluated by Asheesh Kumar and Devesh Kumar [31]. Adsorption of nucleobases adenine, guanine, cytosine, thymine, and uracil over boron nitride, carbon, and magnesium oxide nanostructures using DFT to study the applicability of nanostructures for the sensing of nucleobases [32-34].

Since, MgO nanoparticles have considerable potential in nanomedicine especially in destroy cancer cells and antibacterial agent [21] and from the side, adsorption of biomolecules on metal oxide nanostructures are extremely useful, therefore, the adsorption of uracil on MgO nanotube in polar and non-polar solvents is very valuable. Taking this background into consideration, we are going to perform a systematic DFT study upon the interaction of uracil biomolecule with MgO nanotube to get more in-depth understanding of optoelectronic and structural behavior of the proposed nano-bio interaction system in vacuum and solvent (water and toluene) environments.

2. Computational details

Theoretical computations were carried out using PBE (Perdew-Burke-Ernzerhof) functional [35] with the empirical dispersion correction (PBE-D) and 6–311 + G** basis set as implemented by Gaussian 09 software [36]. The PBE functional has been previously reported to study the MgO nanostructures [37,38]. GaussSum program [39] has been used to get the frontier molecular orbital (FMO) and molecular electrostatic potential (MEP). Multiwfn software package [40] has been applied to get the total density of state (TDOS), projected density of state (PDOS), color-filled maps of electron density (ED), electrostatic population charge analysis (ESP), and electron localization function (ELF) plots. For all studied complexes, the Self Consistent Field (SCF) convergence limit was set to 10^{-6} a.u. over energy and electron density. We also applied the basis set superposition error (BSSE) on adsorption energy for the all studied complexes by the counterpoise method [41]. In addition to the calculations in vacuum phase, the structural and optoelectronic properties of the MgO nanotubes in water (dielectric constant of 78.4 ε) and toluene (dielectric constant of 2.37 ε) were investigated with the polarizable continuum model (PCM) method [42]. No symmetry constraints were carried out during the optimizations. Binding energies (E_b) were calculated using the formula:

$$E_b = E_{Complex} - -\backslash;\left(E_{MgONT} + E_{Uracil}\right) + E_{BSSE} \quad (1)$$

where $E_{Complex}$ is the total energy of MgONT interacting with the uracil molecule. E_{MgONT} is the total energy of the pristine MgONT, and E_{Uracil} is the total energy of an isolated uracil molecule.

Using the previously relaxed structures, UV–VIS electronic absorption spectra were calculated in the vacuum and solvents within the TD-DFT method. A total of 50 excited states for the fragments (MgONT and uracil) and the corresponding complexes were calculated as vertical excitations.

3. Results and discussion

3.1. The structures of uracil and MgONT

The optimized configuration, FMO, MEP plots of uracil in vacuum environment is displayed in Fig. 1. As illustrated in Fig. 1, electron density in the HOMO is dispensed on the uracil ring, with a large amount localized at the O_{10} and O_{12} atoms, while the electron density in the LUMO is distributed on the C-H, N-H, and C = O groups of the molecule. MEP plot of uracil is provided and shown in Fig. 1 to understand possible reaction site. MEP plot represents that the most possible sites for an electrophilic attack (red color) are O_{10} and O_{12} atoms and nucleophilic attack (blue color) are N_4, N_2, and C_5. Fig. 2 displays HOMO and LUMO plots of the MgONT. So that electron densities of the HOMO and the LUMO in turn are mostly localized at the oxygen atoms, and at the magnesium atoms [43].

MgONT indicates a high symmetry of D_{3h} with all ions upon the surface, in which the tube has a length of 8.056 Å with the formula $(MgO)_{15}$. The calculated Mg-O bond length in gas, toluene, and water environments are 1.995, 2.004, and 2.018 Å, respectively (**see** Table 1 and Fig. 3), which are longer than the results reported

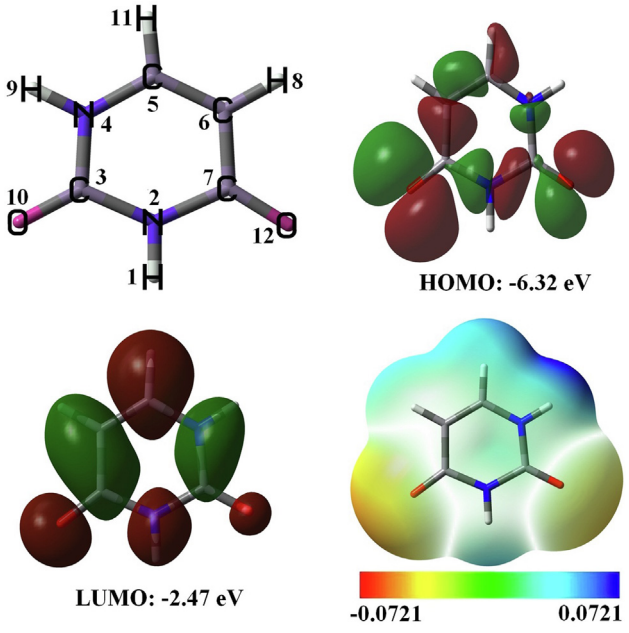

Fig. 1. Optimized structure the uracil molecule and the FMO and MEP plots.

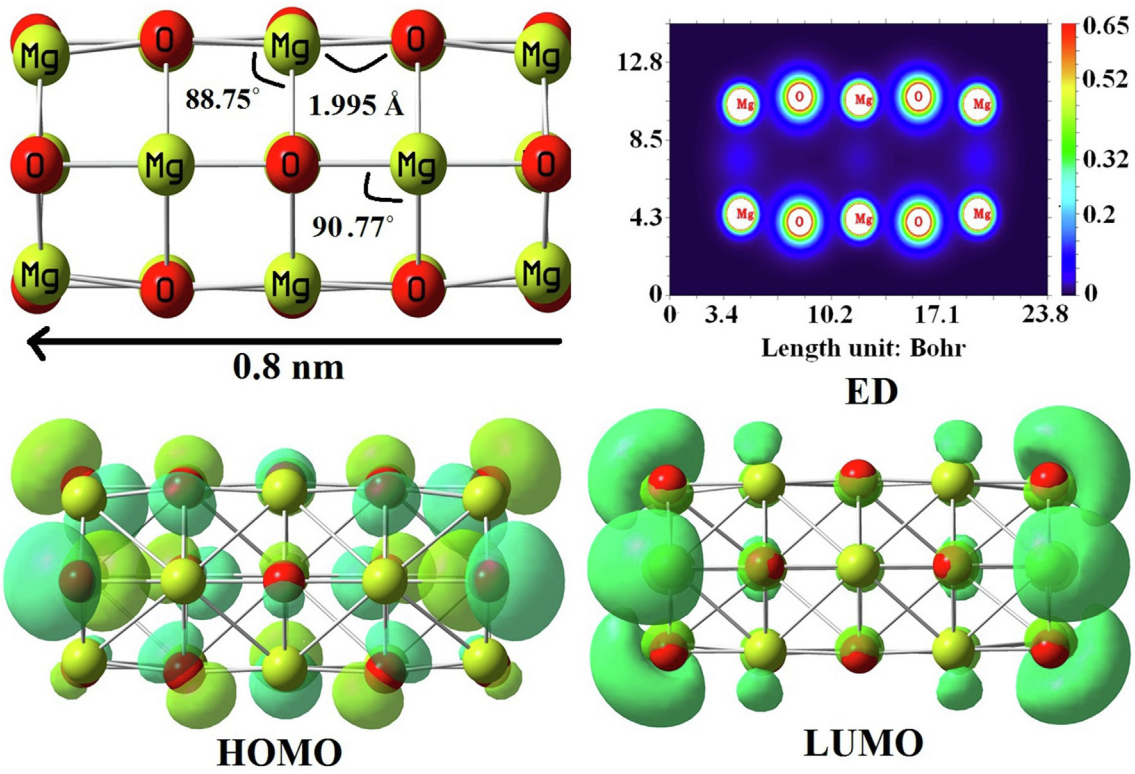

Fig. 2. Optimized structure of MgONT, ED and FMO plots.

Table 1
Calculated the bond length for uracil adsorbed at four different states.

Property	Mg-O/Å	C5-C6/Å	C3-O10/Å	C5-N4/Å	C3-N2/Å	N2-C7/Å	C7-C6/Å	C7-O12/Å	N4-H9/Å	N2-H1/Å
Vacuum										
MgO	1.995	–	–	–	–	–	–	–	–	–
I	2.251	1.371	1.269	1.367	1.379	1.422	1.447	1.231	1.569	1.02
II	2.3	1.37	1.277	1.368	1.376	1.423	1.446	1.231	1.606	1.02
III	2.13	1.356	1.283	1.378	1.333	1.402	1.469	1.237	1.016	1.598
IV	2.067	1.359	1.219	1.375	1.394	1.401	1.446	1.242	1.017	1.021
Water										
MgO	2.018	–	–	–	–	–	–	–	–	–
I	2.216	1.379	1.268	1.358	1.389	1.408	1.437	1.248	1.743	1.021
II	2.235	1.378	1.274	1.36	1.386	1.41	1.437	1.246	1.782	1.021
III	2.095	1.359	1.278	1.371	1.34	1.389	1.461	1.255	1.017	1.826
IV	2.061	1.44	1.223	1.374	1.39	1.4	1.44	1.248	1.018	1.021
Toluene										
MgO	2.003	–	–	–	–	–	–	–	–	–
I	2.243	1.375	1.268	1.363	1.384	1.415	1.442	1.239	1.675	1.02
II	2.273	1.374	1.275	1.364	1.381	1.416	1.442	1.238	1.702	1.02
III	2.118	1.357	1.281	1.375	1.336	1.396	1.466	1.245	1.016	1.698
IV	2.066	1.36	1.223	1.374	1.392	1.401	1.444	1.244	1.017	1.021

by Yang et al. (1.919 Å), whilst the average Mg-O bond length in the end of tube in vacuum, toluene, and water environments are found to be 1.934, 1.948, and 1.965 Å, respectively [38]. Sharma and Kakkar calculated the length of Mg-O bond with a value of 1.909 Å [28]. We considered the four states of uracil adsorption, namely, states **I, II** and **III** with C = O which the oxygen oriented atop a Mg atom and a hydrogen atom of uracil is broken and bonded to oxygen atom in the center and end of tube, and state **IV** with C = O that the oxygen oriented atop a Mg atom in the center and a C-H of molecule close to oxygen atom of the tube. In continue, we calculated the interaction energies between uracil and MgO nanotube in both vacuum and solution (toluene and water) environments as presented in Table 3. It can be seen that the interaction happens between the electron-rich uracil carbonyl group and the electron-poor MgO nanotube with binding energy of −1.864 eV representing a stable chemical bond (chemisorption) in nature between Mg atom of tube and O atom of the molecule in vacuum environment and −1.709 and −1.592 eV in toluene and water environments as the most stable site (**III**). The nearest distance of Uracil-Mg of the tube is 2.174 Å in vacuum environment and is 2.193 and 2.056 Å in toluene and water environments, respectively. Our findings present that the chemisorption of uracil on MgO surface in vacuum environment is slightly more stable than the toluene and water environments. Seino *et al.* have been investigated the electronic properties of uracil-covered Si(0 0 1) surface by using the DFT calculations [14]. They show that the computed binding energies of the uracil from dienol to keto-enol via diffusion of hydrogen are 2.77 **(D-1)** and 3.66 eV **(C-1)** and

Table 2
Calculated the bond angle for uracil adsorbed at four different states.

Property	Mg-O-Mg/°	O-Mg-O/°	N_2-C_3-N_4/°	C_6-C_5-N_4/°	C_5-N_4-C_3/°	C_3-N_2-C_7/°	C_7-C_6-C_5/°	O_{10}-C_3-N_2/°	O_{12}-C_7-N_2/°
Vacuum									
MgO	88.75	90.77	–	–	–	–	–	–	–
I	87.32	85.29	118.9	125.37	117.72	126.48	119.56	118.66	120.04
II	83.4	87.46	119.25	125.4	117.51	126.36	119.58	118.24	119.97
III	88.1	88.55	119.68	120.27	121.18	122.79	119.76	123.87	120.55
IV	88.9	88.92	112.37	121.77	123.97	127.59	119.1	124.3	118.76
Water									
MgO	88.57	90.89	–	–	–	–	–	–	–
I	87.55	86.77	118.85	125.51	117.64	126.11	119.18	118.19	119.74
II	84.32	89.94	119.2	125.53	117.42	125.99	119.2	117.84	119.73
III	87.87	90.26	119.73	119.93	121.55	121.65	119.31	123.88	120.24
IV	89.55	89.16	112.99	121.72	123.76	127.18	119.06	123.57	118.82
Toluene									
MgO	88.86	90.7	–	–	–	–	–	–	–
I	87.47	85.63	118.96	125.58	117.48	126.35	119.37	118.29	119.96
II	83.92	88.03	119.29	125.56	117.32	126.22	119.4	117.95	119.92
III	88.13	89.05	119.74	120.14	121.3	122.28	119.55	123.86	120.44
IV	89.11	89.02	112.67	121.72	123.89	127.4	119.09	124.00	118.8

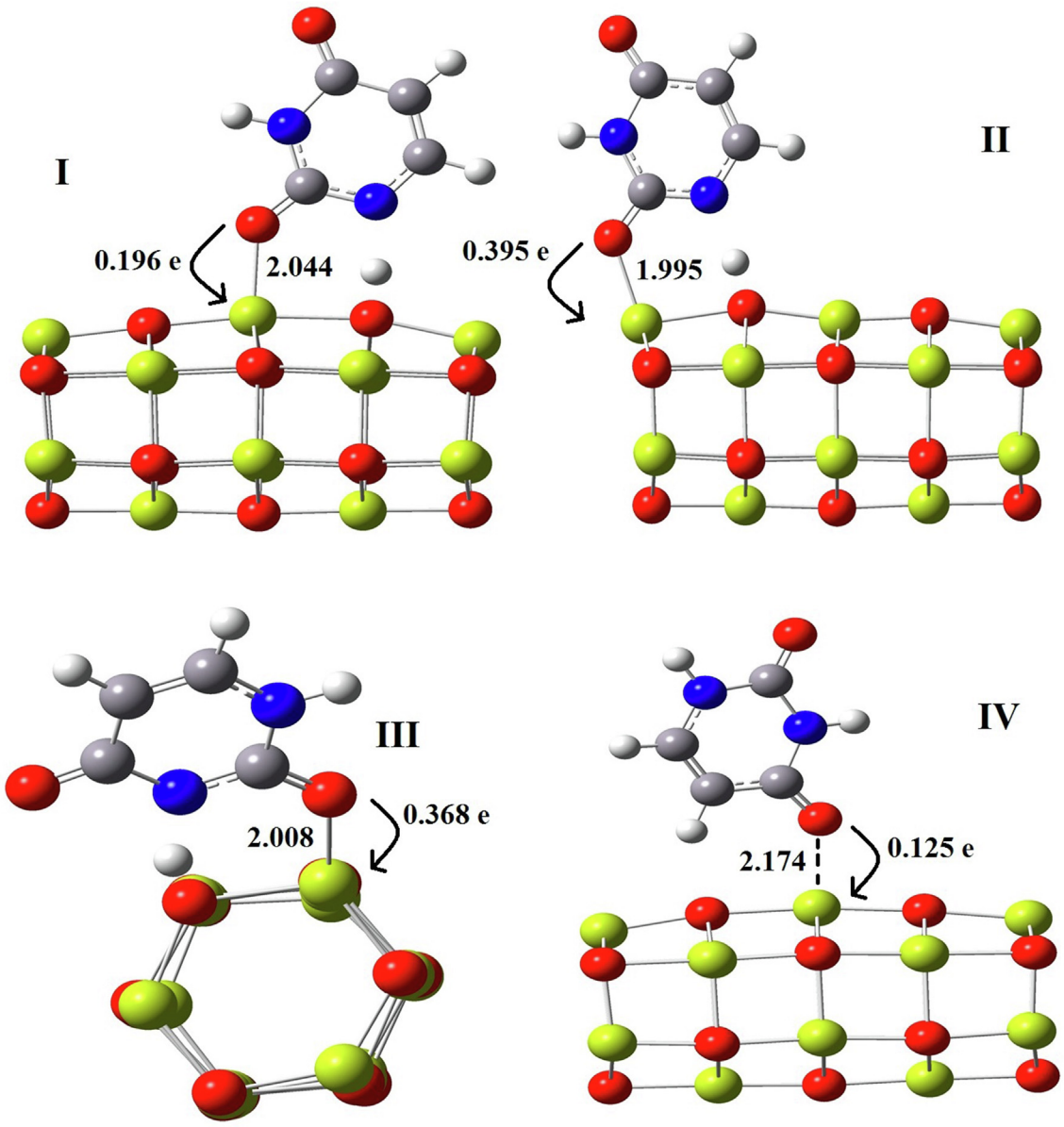

Fig. 3. The relaxed geometry for various states of the uracil/MgO nanotube complexes.

Table 3
Calculated the adsorption energy (E_{ad}/eV), dipol moment (DM/Debye), charge transfer (Q/e), HOMO-LUMO gap (E_g/eV), for uracil adsorbed at four different states.

Property	E_{ad}/eV	D/Á	Q/e	E_{HOMO} /eV	E_{LUMO} /eV	E_g/eV	ΔE_g/%	E_F/eV	DM/Debye
Vacuum									
MgO	–	–	–	−5.27	−2.26	3.01	–	−3.77	0.14
I	−1.101	2.044	0.196	−5.29	−2.63	2.66	11.63	−3.96	9.00
II	−1.626	1.995	0.395	−5.35	−2.55	2.80	6.98	−3.95	9.60
III	−1.864	2.008	0.368	−4.73	−2.27	2.46	27.15	−3.50	3.04
IV	−0.543	2.174	0.125	−4.97	−2.98	1.99	33.89	−3.98	5.43
Water									
MgO	–	–	–	−4.71	−1.47	3.24	–	−3.09	0.04
I	−1.193	2.125	0.176	−4.69	−1.70	2.99	7.72	−3.19	15.66
II	−1.439	2.056	0.254	−4.75	−1.76	2.99	7.72	−3.25	15.12
III	−1.592	2.056	0.351	−4.75	−1.64	3.11	4.01	−3.19	5.25
IV	−0.193	2.233	0.101	−4.65	−2.43	2.22	31.48	−3.54	2.22
Toluene									
MgO	–	–	–	−4.90	−1.77	3.13	–	−3.34	0.03
I	−1.097	2.072	0.154	−4.90	−1.99	2.91	7.03	−3.44	11.84
II	−1.502	2.019	0.277	−5.08	−1.95	3.13	0.0	−3.51	12.50
III	−1.709	2.027	0.373	−4.93	−1.82	3.11	0.64	−3.38	4.80
IV	−0.347	2.193	0.126	−4.74	−2.64	2.10	32.91	−3.69	6.02

the values of binding energies for oxygen insertion into Si dimer are found to be 3.78 **(D-2)** and 5.27 eV **(C-2)**. Irrera *et al.* indicated the adsorption energy of uracil through N_1 deportation over Au (1 1 1) surface (-1.95 eV) which is more stable than interaction on Au(1 0 0) (-1.67 eV) surface [44]. Our results represent that the uracil adsorption at the N_2 position is more possible than other positions, which is close to the study conducted by Li *et al* [45]. When the uracil molecule is adsorbed on the MgO nanotube surface, the local surface structure of the tube is significantly distorted therefore the bond length in the nanotube systems are expanded by a smaller amount and the length of bonds are changed accordingly (**See** Tables 1 and 2). The Mg-O bonds are typically of ionic character in nature and a charge transfer revealed to be happened from Mg (+1.202 e) to more electronegative O (-1.202 e) atoms that is confirmed by electrostatic population charge analysis (ESP) study [46]. Taking all interaction states into account, the largest charge transfer happens at vacuum phase from the uracil to the tube (state **II**: 0.395 e) in comparison with toluene and water environments (**III:** 0.373 and 0.351 e). The values of total electric dipole moment (DM) in Debye, Table 3, show that the intra-charge fluctuation comprised of a strong conversion of the electric dipole of the system between the vacuum or solution environment and the adsorption states. The dipole moment value for free MgO nanotube is calculated with the amounts of 0.137, 0.0284, and 0.044 Debye in vacuum, toluene, and water environments, respectively. Expect the state **IV** in water environment, in all remaining states at two environments (vacuum and toluene), the dipole moment values underwent a reduction trend as binding energy values. Upon uracil adsorption on the nanotube surface, the binding energy in the state **III** increased as the most stable state, since the value of dipole moment is reduced after interaction process as 3.04 (vacuum), 4.08 (toluene), and 5.25 Debye (water).

3.2. PDOS and FMO analysis

The discrepancy of energy between highest occupied molecular orbital (HOMO) and lowest unoccupied molecular orbital (LUMO) were obtained from the TDOS results (**See** Table 3). The HOMO and LUMO analysis demonstrate that the charge transfer occur within the MgO nanotube. In the charge distribution, HOMO orbital with the positive phase functions as an electron donor while the LUMO with the negative phase that largely functions as the electron acceptor [15]. Fig. 4 shows the molecular energy levels of the studied structures in the most stable state. In the most stable state, **III**, the values of HOMO, HOMO-3, and HOMO-10 wave functions are calculated to be −4.73, −5.29, and −5.69 eV, whereas the values of LUMO, LUMO + 3, and LUMO + 10 wave functions are found to be −2.27, −1.19, and −0.07 eV, respectively. It can be seen in the results that the HOMO wave function was mainly localized on uracil, whereas the LUMO wave function was mostly localized on Mg and O atoms of the nanotube**.** The distribution of the wave function on the molecular structure shows the chemical active points. The result represents HOMO-3 and LUMO + 10 electron distribution plots that significantly altered after the uracil interacting over the surface of the MgO nanotube.

Experimental band gap energies of MgONT have been calculated to be 0.3 to 7.1 eV [47,48] and Pathak *et al.* calculated the E_g value of 5.09 eV using DFT-PBE calculations [49]. As presented in Table 3, E_g value in MgO nanotube decreased from 3.01 eV (vacuum), 3.13 eV (toluene), and 3.24 eV (water) to 1.99, 2.10, and 2.22 eV after the uracil adsorbing to the surface of the MgO nanotube, respectively, while state **IV** have more changes in both vacuum and solvent phases with the values of 33.89 (vacuum), 32.91% (toluene), and 31.48% (water). Considering the TDOS plots in both environments (Fig. 5), a shift of bonds to lower energy as the result of uracil interaction with the MgO nanotube. However, a decrement in the E_g between the valence band and the conduction band is clearly apparent from TDOS plots. The PDOS plots of first (MgO) and the second (uracil) fragments are demonstrated as red and blue colors of the determined complexes. The PDOS curve in Fig. 5 display that the uracil in the state **IV** presents certain impurity states in the E_g and creates localized states near the Fermi level (E_F), hence, uracil adsorption on MgO nanotube will diminish the original E_g. From the present calculations we found that the uracil adsorption affects the electronic properties and the results demonstrated that the change of energy gap in vacuum environment for the state **IV** becoming slightly larger than other states in the toluene and water environments. These results are in well agreement with previous reports over the functionalization of the MgO nanostructures' surfaces with biomolecules which changes in the electronic structure of the MgO nanostructures are clear [50]. The charge distribution can be evaluated by molecular electrostatic potential (MEP) plots. As demonstrated by the MEP maps of MgONT in Fig. 6, the Mg (charge-donating) and O (charge-withdrawing) atoms with blue and red colors are positively and negatively charged and it reveals that a large charge transfer is occurred from Mg atoms to the O atoms give raise to a strong ionic bonding in the surface of the tube. Furthermore, Fig. 6 demonstrates that the oxygen atom of the adsorbed uracil is more negative (with a charge of −0.837 e) than its hydrogen atom (with a

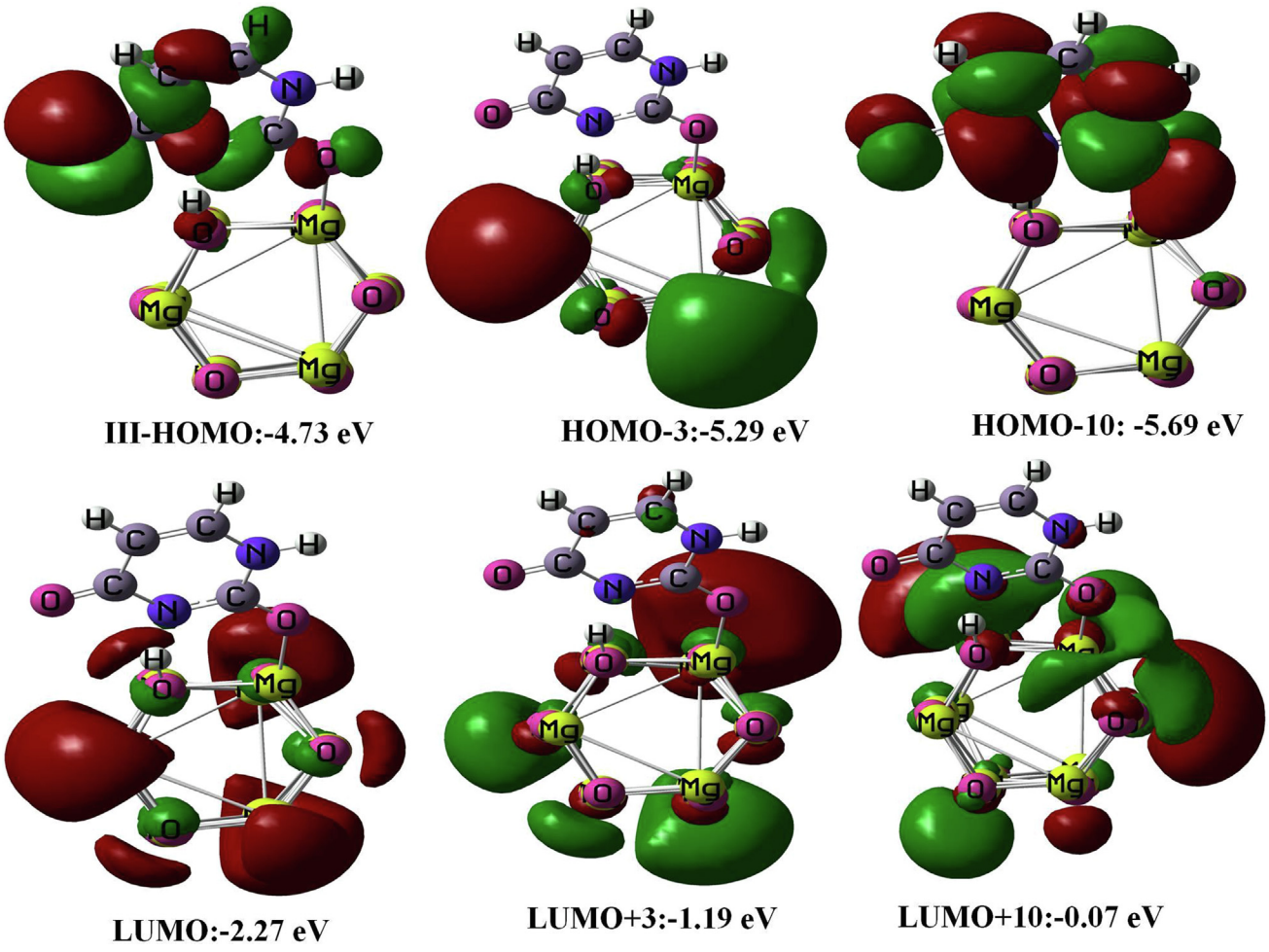

Fig. 4. Contour plots of HOMO and LUMO for the uracil/MgO nanotube complexe.

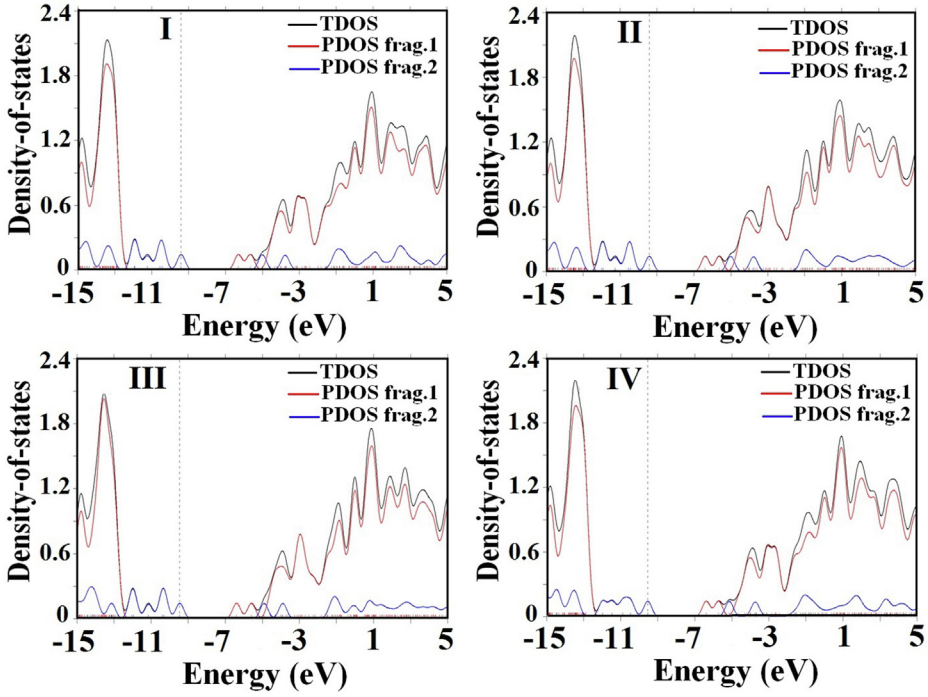

Fig. 5. Computed PDOS plots for the most stable states of uracil/MgO nanotube complexes.

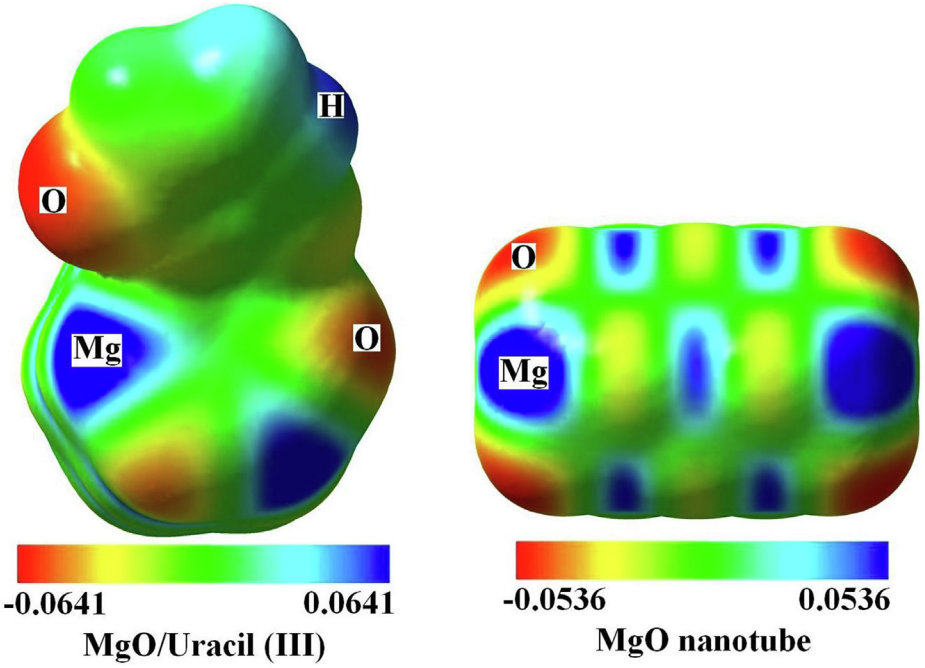

Fig. 6. The molecular electrostatic potential plot of the uracil molecule interacting with the MgO nanotube.

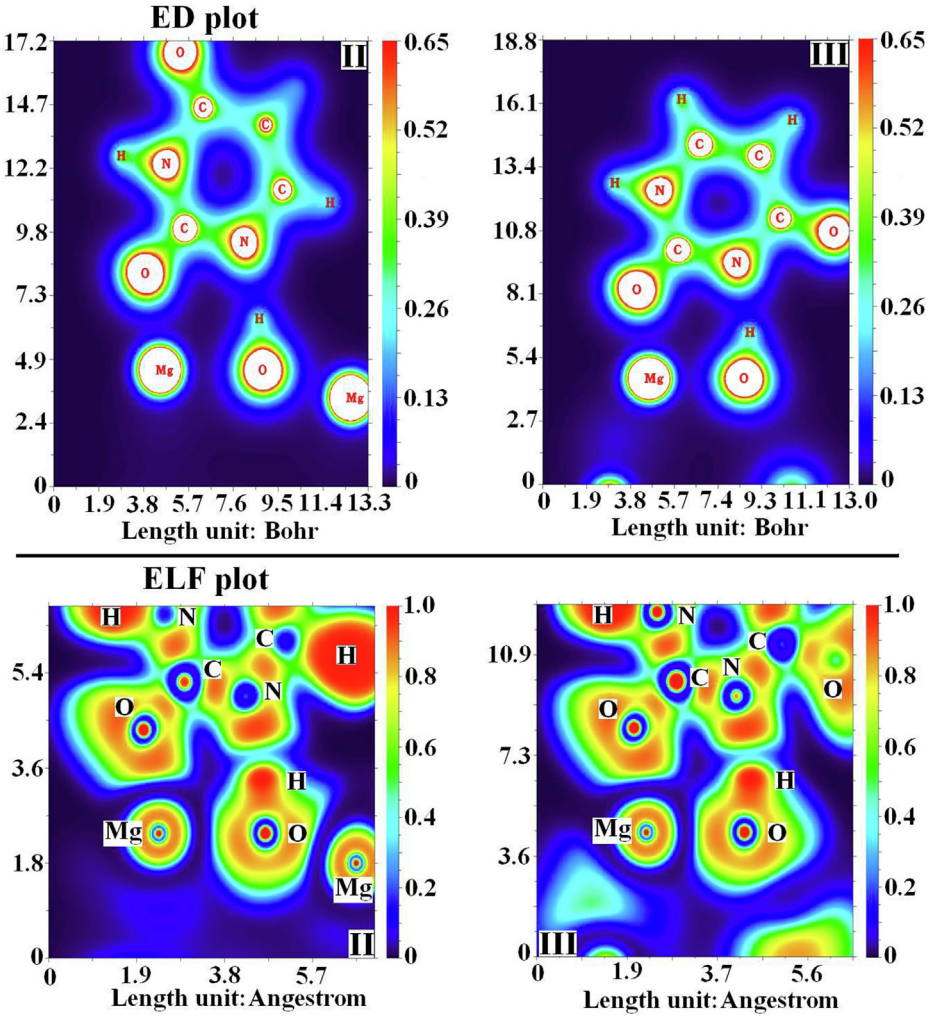

Fig. 7. Color-filled maps of electron density and electron localization function plots of the uracil/MgO nanotube complexes.

charge of + 0.448 e in vacuum environment) compared with the electron poor Mg atom of the tube with a positive charge of + 1.646 e. Thereby, the calculated charge of adsorbed uracil is more positive confirming a charge transfer from uracil to the nanotube by means of a strong interaction. Fig. 7 shows color-filled maps of electron density (ED) and electron localization function (ELF) plots for the uracil/MgONT complex in the most stable states (**II** and **III**). One can see a substantial localization (red areas) between the oxygen and hydrogen atoms of the uracile and the Mg and oxygen atoms of the MgONT leading to a strong covalent

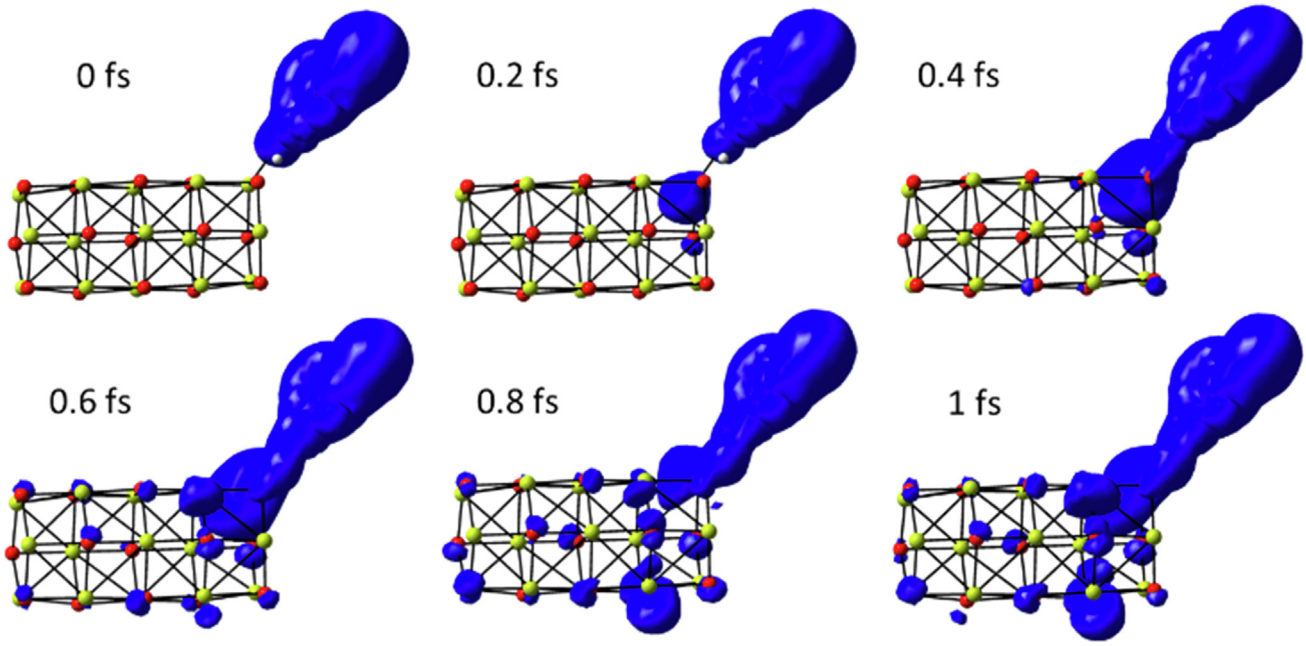

Fig. 8. Evolution of time-dependent charge distribution during the early time relaxation dynamics after instantaneously populating the uracil molecule upon the MgO nanotube.

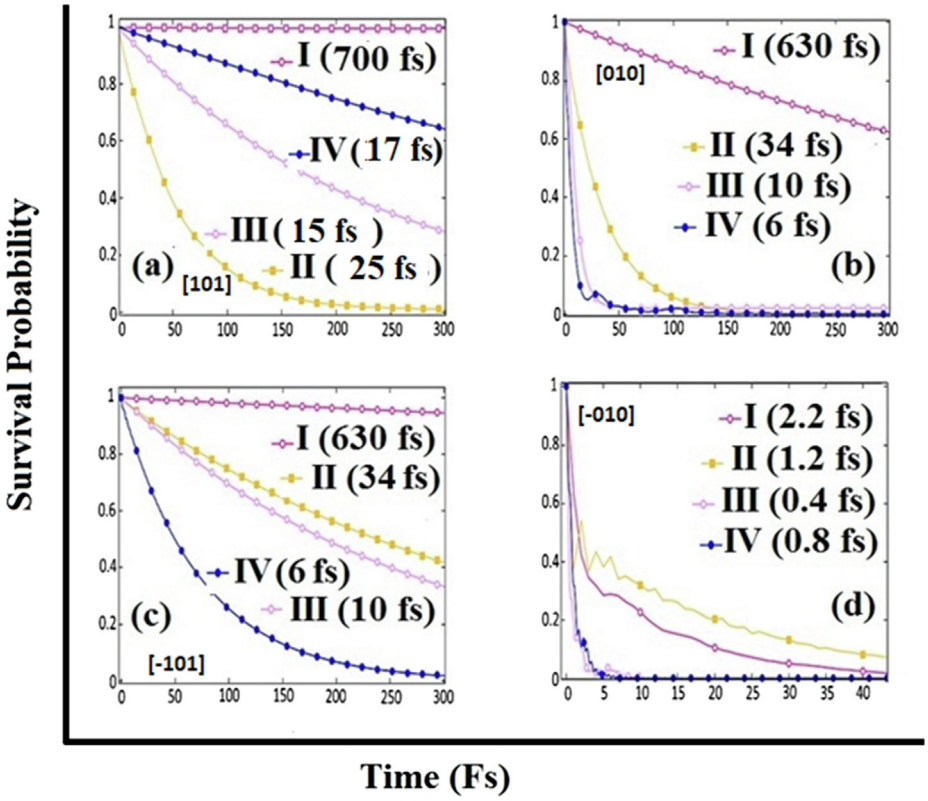

Fig. 9. Time-dependent survival probability in a sensitized uracil/MgONT system. The dashed lines are the exponential fitting curves to the four elementary steps for electron transfer in the complexes.

interaction in the states **I**, **II**, and **III**, respectively. ED plots in Fig. 7 visibly demonstrated a strong interaction because of the charge transfer from the uracil to the MgONT in the states **II** and **III**, since we made obvious the electrostatic interaction in the state **IV**.

We reported the photoinjection mechanisms from the excited electronic states of adsorbed uracil over the surface of MgONT. The photoexcitation of MgONTs surface can cause to interfacial electron transfer when there is an appropriate energy match between the photoexcited electronic state in the MgONTs surface and the electronic states in the E_g of the MgONT. Fig. 8 demonstrates the comparison of electron injection times as short as a few femtoseconds for uracil-LUMO into the MgONT. Fig. 9 illustrates electron injection times until the injected charge reaches in the edge of MgONT. In fact, the temporal evolution of the charge distribution and its expansion due to the interaction of the uracil molecule with the MgO nanotube is illustrated in Figs. 8 and 9. It describes the survival probability as it describes electrons remaining probability on the uracil molecule during time due to this interaction. Fig. 8 shows the charge injection in terms of time in the order of femtoseconds for II configuration. As is clear, the charge is injected over the nanotube along [1 0 1] direction, although most of the charge remains on the uracil molecule within 1 fs. The rest time for remaining charge on the uracil is displayed in various configurations in the Fig. 9 for [1 0 1], [0 1 0], [−1 0 1], and [−0 1 0] direction. There are significant changes in relaxation time of the injection for different configurations. The relaxation time of the charge on the uracil molecule is displayed in parentheses for a variety of configurations. In addition, we can see the direction of the charge injection and charge distribution on the nanotube surface is effective at relaxation time. For example, charge injection occurs quickly in some cases compared to others. In the [−0 1 0] direction, for III configuration we see an ultra-fast injection of the charge about 0.4 fs, which is very significant. In contrast, in the [1 0 1] direction of the II configuration, the charge injection takes up to 700 fs.

3.3. UV–Vis spectroscopy analysis

According to the obtained results in Table 4, the TDDFT calculation of excitation wavelengths (λ_{max}) was carried out for the uracil-MgONT system in various states. Based on TDDFT calculation, the excitation energy (E) of MgONT is calculated to be 4.634 eV in the region of 267 nm with oscillator strength (*f*) of 0.0518. According to the experimental results, the absorption band of the MgO nano-particle was found to be 220–650 nm through UV/Vis spectroscopy [51]. The UV/Vis spectrum can well determine the optical gap of the studied samples and thus provide an estimate for the experimental agreement. The states of the absorption edge are therefore decisive in determining the optical gap. In vacuum mode, the optical gap the modes **I** to **IV** are equal to 4.598, 4.659, 4.573, and 4.653 eV, respectively. The values of the optical gap clearly show that modes **II** and **IV** are not much different in terms of optical gap. In addition, both major contributions to the excitation of molecular levels are related to the excitation of the H-3 level to

Table 4
Optical properties of the uracil interacting with MgONT calculated in different environments.

Methods	Energy/eV	λ_{max}/nm	*f*	Assignment
Vacuum				
	4.598	269.63	0.0243	H-1 → L (10%), H-1 → L + 1 (63%)
I	4.617	268.49	0.0034	H → L (67%), H → L + 2 (20%)
	4.673	265.32	0.0227	H-10 → L (32%), H-7 → L (19%), H-6-→L (15%)
II	4.659	266.08	0.0242	H-3 → L (62%), H-3 → L + 1 (-13%)
	4.683	264.7	0.0243	H-4 → L (62%), H-4 → L + 1 (-13%)
	4.744	261.33	0.0396	H-2 → L (10%), H-2 → L + 1 (21%), H-1 → L (17%), H-1 → L + 1 (30%)
III	4.573	271.08	0.0138	H → L + 1 (17%), H → L + 2 (49%)
	4.581	270.62	0.0323	H-5 → L + 1 (18%), H-4 → L + 1 (19%), H-3 → L + 1 (12%)
	4.592	269.97	0.0149	H-1 → L + 1 (14%), H-1 → L + 2 (46%)
IV	4.653	266.41	0.0236	H-3 → L (27%), H-3 → L + 1 (11%), H-2 → L (28%), H-2 → L + 1 (12%)
	4.655	266.29	0.025	H-3 → L (28%), H-3 → L + 1 (-11%), H-2 → L (27%), H-2 → L + 1 (10%)
	4.696	263.97	0.0257	H-1 → L (27%), H-1 → L + 1 (25%)
Toluene				
	4.407	281.34	0.0013	H → L (72%), H → L + 2 (20%)
I	4.493	275.93	0.0263	H-1 → L + 1 (64%)
	4.522	274.15	0.0273	H-2 → L + 1 (61%)
II	4.556	272.12	0.0242	H-3 → L (62%), H-3 → L + 1 (13%)
	4.577	270.88	0.0243	H-4 → L (61%), H-4 → L + 1 (13%)
	4.641	267.14	0.0387	H-2 → L (12%), H-2 → L + 1 (27%), H-1 → L (13%), H-1 → L + 1 (25%)
III	4.472	277.21	0.0013	H → L + 2 (32%)
	4.476	276.98	0.0448	H-4 → L + 1 (11%), H → L + 2 (24%)
	4.493	275.92	0.0124	H-6 → L + 1 (11%), H-4 → L + 1 (-14%), H-2 → L + 1 (25%)
IV	4.55	272.47	0.0227	H-4 → L (22%), H-4 → L + 1 (13%), H-3 → L(26%), H-3 → L + 1 (15%)
	4.551	272.38	0.0229	H-4 → L (25%), H-4 → L + 1 (16%), H-3 → L (22%), H-3 → L + 1 (14%)
	4.572	271.14	0.0273	H-1 → L (27%), H-1 → L + 1 (17%)
Water				
I	4.132	300.04	0.0011	H → L (76%), H → L + 2 (16%)
	4.407	281.31	0.0266	H-2 → L + 1 (10%), H-1 → L + 1 (53%)
	4.422	280.34	0.0270	H-2 → L + 1 (51%)
II	4.481	276.64	0.0255	H-4 → L (58%), H-4 → L + 1 (14%)
	4.507	275.05	0.0251	H-5 → L (62%), H-5 → L + 1 (14%)
	4.567	271.43	0.0420	H-3 → L (12%), H-3 → L + 1 (30%), H-1 → L (10%), H-1 → L + 1 (20%)
III	4.372	283.53	0.0179	H-5 → L + 1 (34%), H-3 → L + 1 (11%)
	4.392	282.27	0.0291	H → L + 1 (12%), H → L + 2 (59%)
	4.414	280.84	0.0198	H-7 → L + 1 (14%), H-2 → L + 1 (10%), H-1 → L + 2(16%)
IV	4.453	278.41	0.0139	H-8 → L (11%), H-2 → L (27%)
	4.465	277.67	0.0220	H-4 → L (27%), H-4 → L + 1 (38%)
	4.466	277.57	0.0283	H-3 → L (28%), H-3 → L + 1 (39%)

the L, L + 1 levels. The difference between the HOMO-LUMO gap in these cases and the optical gap indicates the energy of the created excitons. The values of the optical gap in the vacuum-based sample in states I to IV are in turn equal to 1.929, 1.589, 2.113 and 2.663 eV. Accordingly, the main difference between the mentioned states, especially states **II** and **IV**, is the difference between the dependence energies of the excitons that are generated, so that at higher dependence energies related to sample **IV**, the recombination of the excitons can create shorter wavelengths and a blue shift in the energy spectrum of the excitons. There are similar conditions for the toluene and water mediums, so that the optical gap for both is significantly reduced compared to the vacuum sample. In the case of water, the optical gap is less than in the case of the similar case for the toluene sample, so a red shift in the optical gap can be described in these cases relative to the vacuum. According to the data in Table 3, the HOMO-LUMO energy gap has increased significantly in toluene and water based samples. As a consequence, the difference between the optical gap and the HOMO-LUMO gap is also grows and makes more localized excitons.

4. Conclusions

We have checked the adsorption behavior of the uracil molecule on the MgO nanotube with density functional theory (DFT) and generalized gradient approximation (GGA) calculations within vacuum, water, and toluene environments. Main focuses have been placed on the binding energy; charge transfer, structural, optical, and electronic properties of the states **II** and **III** as the most stable adsorption configurations compared to other studied states. It was found that the uracil was strongly interacted with the surface of MgO nanotube with higher reactivity over the end of MgO nanotube in comparison with the center in which the oxygen atom of uracil prefers to interact to the Mg atom of the nanotube in vacuum environment in contrast with water and toluene environments. The adsorption of uracil in state **IV** causes a small distortion of the nanotube structure while greatly widening its energy gap.

CRediT authorship contribution statement

Yan Cao: Resources, Software, Funding acquisition. **Afrasyab Khan:** Data curation, Methodology. **M. Javan:** Methodology, Project administration. **Mohammad T. Baei:** Writing - review & editing, Investigation. **Elham Tazikeh-Lemeski:** Formal analysis, Software. **Zivar Azmoodeh:** Resources, Writing - original draft, Project administration. **Alireza Soltani:** Conceptualization, Data curation, Formal analysis, Investigation, Software, Supervision. **Fatemeh Heidari:** Writing - original draft, Validation, Formal analysis. **Marieh Pishnamazi:** Validation, Writing - original draft. **Ahmad B. Albadarin:** Supervision, Writing - review & editing, Resources, Formal analysis.

Declaration of Competing Interest

The authors declare that they have no known competing financial interests or personal relationships that could have appeared to influence the work reported in this paper.

Acknowledgements

We would like to thank the clinical Research Development Unit (CRDU), Sayad Shirazi Hospital, Golestan University of Medical Sciences, Gorgan, Iran.

The authors are thankful to the Russian Government and Institute of Engineering and Technology, Department of Hydraulics and Hydraulic and Pneumatic Systems, South Ural State University, Lenin prospect 76, Chelyabinsk, 454080, Russian Federation for their support to this work through Act 211 Government of the Russian Federation, contract No. 02. A03.21.0011.

References

[1] C.T. Campbell, Surf. Sci. Rep. 27 (1997) 1–111.
[2] C.T. Campbell, A.W. Grant, D.E. Starr, S.C. Parker, V.A. Bondzie, Top. Catal. 14 (2001) 43–51.
[3] M. Baumer, H.J. Freund, Prog. Surf. Sci. 61 (1999) 127–198.
[4] W.T. Wallace, B.K. Min, Top. Catal. 34 (2005) 17–30.
[5] C.R. Henry, Surf. Sci. Rep. 31 (1998) 235–325.
[6] T.P. St Clair, D.W. Goodman, Top. Catal. 13 (2000) 5–19.
[7] X. Liu, F. Wang, R. Aizen, O. Yehezkeli, I. Willner, J. Am. Chem. Soc. 135 (2013) 11832–11839.
[8] Y. Lu, B.R. Goldsmith, N.J. Kybert, A.T.C. Johnson, Appl. Phys. Lett. 97 (2010) 083107.
[9] H. Chang, L. Tang, Y. Wang, J. Jiang, J. Li, Anal. Chem. 82 (2010) 2341–2346.
[10] S. He, B. Song, D. Li, C. Zhu, W. Qi, Y. Wen, L. Wang, S. Song, H. Fang, C.A. Fan, Adv. Funct. Mater. 20 (2010) 453–459.
[11] T.A. Hilder, J.M. Hill, Small 5 (2009) 300–308.
[12] Z. Jin, W. Sun, Y. Ke, C.J. Shih, G.L. Paulus, Q. Hua Wang, B. Mu, P. Yin, M.S. Strano, Nat. Commun. 4 (2013) 1663.
[13] J. Prasongkit, A. Grigoriev, B. Pathak, R. Ahuja, R.H. Scheicher, J. Phys. Chem. C 117 (2013) 15421–15428.
[14] K. Seino, W.G. Schmidt, F. Bechstedt, PHYSICAL REVIEW B 69 (2004) 245309.
[15] V.L. Chandraboss, B. Karthikeyan, S. Senthilvelan, Phys. Chem. Chem. Phys. 16 (2014) 23461–23475.
[16] S. Saha, P. Sarkar, Phys. Chem. Chem. Phys. 16 (2014) 15355–15366.
[17] J. Gunster, G. Liu, J. Stultz, S. Krischok, D.W. Goodman, J. Phys. Chem. B 104 (2000) 5738–5743.
[18] D. Costa, C. Chizallet, B. Ealet, J. Goniakowski, F. Finocchi, J. Chem. Phys. 125 (2006) 054702.
[19] G. Pacchioni, J.M. Ricart, F. Illas, J. Am. Chem. Soc. 116 (1994) 10152–10158.
[20] R.S. Kumaran, Y.-K. Choi, V. Singh, H.-J. Song, K.-G. Song, K.J. Kim, H.J. Kim, Int. J. Mol. Sci. 16 (2015) 7551–7564.
[21] D.R. Di, Z.Z. He, Z.Q. Sun, J. Liu, Nanomedicine 8 (2012) 1233–1241.
[22] M.K. Patel, V.V. Agrawal, B.D. Malhotra, S.G. Ansari, Mater. Focus 3 (2014) 1–11.
[23] L. Zhu, R. Zhao, K. Wang, H. Xiang, Z. Shang, W. Sun, Sensors 8 (2008) 5649.
[24] K. Karthikeyan, J.Y. Moon, H.B. Hyun, S.K. Cho, S.J. Kim, J. Mater. Chem. 22 (2012) 24610.
[25] T. Fornaro, J. Robert Brucato, S. Branciamore, A. Pucci, Int. J. Astrobiol. 12 (1) (2013) 78–86.
[26] M. Rajarajeswari, K. Iyakutti, Y. Kawazoe, Phys. Status Solidi B 248 (2011) 1431–1436.
[27] M.T. Baei, M. Ramezani Taghartapeh, E. Tazikeh Lemeski, A. Soltani, Phys. B 444 (2014) 6–13.
[28] N. Sharma, R. Kakkar, J. Comput. Sci. 10 (2015) 225–236.
[29] M. Yang, Y. Zhang, S. Huang, H. Liu, P. Wang, H. Tian, Appli, Surf. Sci. 258 (2011) 1429–1436.
[30] S. Gowtham, R.H. Scheicher, R. Pandey, S.P. Karna, R. Ahuja, Nanotechnology 19 (2008) 125701.
[31] A. Kumar, D. Kumar, J. Molecu. Struct. 1222 (2020) 128889.
[32] S.D. Dabhi, B. Roondhe, P.K. Jha, Phys. Chem. Chem. Phys. 20 (2018) 8943–8950.
[33] A. Shokuhi Rad, S.M. Aghaei, E. Aali, M. Peyravi, M. Jahanshahi, Appl Organometal Chem. 32 (2017) e4070.
[34] T. Fornaro, J.R. Brucato, S. Branciamore, A. Pucci, Int. J. Astrobiol. 12 (2013) 78–86.
[35] J.P. Perdew, K. Burke, M. Ernzerhof, Phys. Rev. Lett. 77 (1996) 3865.
[36] M.W. Schmidt, K.K. Baldridge, J.A. Boatz, S.T. Elbert, M.S. Gordon, J.H. Jensen, S. Koseki, N. Matsunaga, K.A. Nguyen, S.J. Su, T.L. Windus, M. Dupuis, J.A. Montgomery, General atomic and molecular electronic structure system, J. Comput. Chem. 14 (1993) 1347–1363.
[37] S.-F. Wang, L.-Y. Chen, T. Zhang, Y. Xie, Physica E 76 (2016) 135–139.
[38] M. Yang, Y. Zhang, S. Huang, H. Liu, P. Wang, H. Tian, Appl. Surf. Sci. 258 (2011) 1429–1436.
[39] N.M. O'Boyle, A.L. Tenderholt, K.M. Langner, J. Comp. Chem. 29 (2008) 839–845.
[40] T. Lu, F. Chen, J. Comput. Chem. 33 (2012) 580–592.
[41] F. Tournus, J.C. Charlier, Phys. Rev. B 71 (2005) 165421.
[42] E. Cances, B. Mennucci, J. Tomasi, J. Chem. Phys. 107 (1997) 3032–3041.
[43] A. Soltani, M. Ramezani Taghartapeh, M. Bezi Javan, P.J. Mahon, Z. Azmoodeh, E. Tazikeh Lemeski, I.V. Kityk, Phys. E 97 (2018) 239–249.
[44] S. Irrera, G. Portalone, N.H. De Leeuw, Surf. Sci. 614 (2013) 20–23.
[45] W.H. Li, W. Haiss, S. Floate, R.J. Nichols, Langmuir 15 (1999) 4875.
[46] M. Moradi, Monatshefte für Chemie - Chemical Monthly 146 (2015) 1613–1619.

[47] A. Moses Ezhil Raj, L.C. Nehru, M. Jayachandran, C. Sanjeeviraja, Cryst. Res. Technol. 42 (2007) 867.
[48] J. Goniakowski, C. Noguera, Surf. Sci. 340 (1995) 191.
[49] N. Pathak, P. Sarathi Ghosh, S. Kumar Gupta, R. Mahadeo Kadam, A. Arya, RSC Adv. 6 (2016) 96398.
[50] D. Scuderi, A. Paladini, M. Satta, D. Catone, S. Piccirillo, M. Speranza, A. Giardini Guidoni, Phys. Chem. Chem. Phys. 4 (2002) 4999.
[51] L. Aghebati-maleki, B. Salehi, R. Behfar, H. Saeidmanesh, F. Ahmadian, Int. J. Electrochem. Sci. 9 (2014) 257.